The modeling of keyhole digging during ablative laser beam interaction with aluminum/magnesium joint

I. Tomashchuk[1]*, M. Mostafa[2,3], P. Sallamand[1], M. Duband[1]

[1] Laboratoire Interdisciplinaire Carnot de Bourgogne (ICB), UMR CNRS 6303 - Université de Bourgogne – Franche Comté, 12, rue de la Fonderie – 71200 Le Creusot, France
[2]Physics Department, College of Science, Jouf University, Sakaka, Saudi Arabia
[3] Laser Tech & Environment Lab, Faculty of Science, South Valley University, 83523- Quena, Egypt
* iryna.tomashchuk@u-bourgogne.fr

Abstract: A lateral observation of laser-induced keyhole through the quartz window is an easy and cheap experimental method. It opens an interesting perspective for the study of keyhole asymmetry in case of dissimilar metal combinations. To quantify the effect of quartz window on the observed phenomena and to predict the keyhole shapes observed in aluminum/magnesium interface, a simplified 2D model of thermal ablation was developed. The main numerical achievement of this work consists in the simulation of keyhole with high depth to width ratio thanks to the adaptive mesh stiffening used in deformed geometry formulation. The model was able to correctly reproduce the keyhole dimensions in case of homogenous and binary metal/quartz combinations and allowed estimating the effect of quartz on the keyhole depth. In case of aluminum/magnesium metal combination, the model renders the keyhole evolution with laser offset from the joint line that would take place in absence of quartz window. In case of the beam centered on the joint line, the mismatch in vaporization temperatures induced the preferential formation of deep and thin keyhole on magnesium side. The displacement of the keyhole on magnesium induced further slight increase of penetration, when the displacement on aluminum reduced abruptly the keyhole.

Keywords: laser, dissimilar joint, heat transfer, deformed geometry.

1. Introduction

During the dissimilar welding of metals with high power laser sources, the mismatch in their physical properties can lead to an asymmetry of the keyhole, which produces a strong effect on shape and composition of the melted zone [1,2]. Very few experimental studies were focused on observation of such keyhole asymmetry. However, this phenomenon was indirectly confirmed by the observable offset of the melted zone root from the joint line, visible on weld cross-sections of some partial penetration welds. Such offset of the root was observed in two cases: between the metals having a strong mismatch in vaporization temperature, such as titanium/tantalum [2], and in the case of strong reflectivity of one of materials, such as copper in copper/steel joints [3]. Torkamany et al [1], proved the keyhole asymmetry during niobium/titanium laser welding using top observation by high-speed camera and metallographic cross-section examination: the keyhole was fully shifted on titanium side. Mostafa et al [4,5] performed an online lateral view observation of the keyhole formed at the joint plane between aluminum A5754 and magnesium AZ31 alloys during a standalone laser pulse using a quartz window transparent to visible and laser radiation. In this configuration, the half of the beam was positioned on the metal joints and the other half passed through the quartz sheet, which allowed approaching the plane symmetry condition of keyhole observation. The experiment was performed in the conditions close to the drilling regime, when the formation of several mm deep keyhole surrounded by a thin liquid layer could be easily observed by high-speed camera. In case of laser beam centered on the joint line, the keyhole was mainly developing on magnesium side having a lower vaporization temperature. Its volume and penetration were slightly modified by the beam shift on magnesium side and were strongly reduced by the beam shift towards aluminum. Taking in account close absorption coefficients of aluminum and magnesium alloys, it was supposed that the mismatch in vaporization temperature is the main factor of keyhole asymmetry. The contact with quartz window is supposed to affect the dimensions of the keyhole, however it provided the possibility to observe the inside of the keyhole at relatively low cost, compared to X-ray imagery [6].

The present article describes a simplified 2D model of laser keyhole digging that reproduces the experiment of Mostafa et al [4] with aluminum/magnesium joint. The additional experiments and calculations of individual metal/quartz combinations were performed to appreciate the effect of the quartz on keyhole digging in the individual materials and the formation of the keyhole on the quartz side. The main numerical achievement of this work consists in the simulation of keyhole with high depth to width ratio thanks to the adaptive mesh stiffening used in deformed geometry formulation.

2. Governing equations

2.1. Heat transfer

The present model was inspired by the COMSOL example ID46671 “Modeling Material Removal through Thermal ablation” described in COMSOL blog article of W. Frei [7]. The time-dependent heat equation was solved over 8 mm high and 4 mm wide rectangular domain created in 2D (**Figure 1a**):

$$\rho\, C_p^{eq} \frac{\partial T}{\partial t} = \overrightarrow{\nabla}\cdot\left(k\,\overrightarrow{\nabla} T\right) \quad (1)$$

with ρ -local density (kg·m^{-3}), C_p^{eq} – local equivalent heat capacity (J·kg^{-1}·K^{-1}), k – thermal conductivity (W·m^{-1}·K^{-1}), T – solved temperature (K) and t – time (s).

The energy supply from laser beam was introduced as Gaussian heat source:

$$q_{laser} = \frac{2\,a\,P}{\pi\,R^2} exp^{-2\frac{(x-\Delta)^2}{R^2}} \cdot \left(t \geq t_{imp}\right) \quad (2)$$

with a – local absorption coefficient of laser radiation, P – laser power (W), R – laser beam radius (m), Δ - laser beam offset from joint line (µm) and t_{imp} – the duration of laser pulse (ms).

The heat loss through evaporation was represented by ablative heat flux:

$$q_{evap} = h(T_{vap} - T) \quad (3)$$

with T-dependent heat transfer coefficient h (W·m^{-2}·K^{-1}) was equal to zero under $T < T_{vap}$ and increased linearly using a ramp function with $1{\cdot}10^9$ slope when $T > T_{vap}$:

$$h = ramp(T - T_{vap}) \quad (4).$$

Thermal insulation was applied to the lateral sides of calculated domain, and ambient temperature was considered for the bottom limit.

The convective movements associated to the expulsion of the liquid metals were neglected to lighten the calculation and avoid the complex displacements of strongly elongated liquid jets that were observed by high-speed imaging (HSI) [4].

2.2. Material properties

To avoid the necessity to squeeze the vertical boundary between two joined materials during the mesh displacement, the domain contained no internal boundaries. The change of physical properties (such as vaporization temperature T_{vap}, laser absorption coefficient a, density ρ, equivalent heat capacity C_p^{eq} and thermal conductivity k) across the joint line was programmed using smoothed Heaviside functions that vertically divide the domain in two equal parts corresponding to the material 1 and material 2:

$$\begin{aligned} T_{vap} &= T_{vap_1} + \left(T_{vap_2} - T_{vap_1}\right) flc2hs(0 - x, dx) \\ a &= a_1 + (a_2 - a_1)\, flc2hs(0 - x, dx) \\ \rho &= \rho_1 + (\rho_2 - \rho_1)\, flc2hs(0 - x, dx) \\ C_p^{eq} &= C_p^{eq}{}_1 + \left(C_p^{eq}{}_2 - C_p^{eq}{}_1\right) flc2hs(0 - x, dx) \\ k &= k_1 + (k_2 - k_1)\, flc2hs(0 - x, dx) \end{aligned} \quad (5)$$

The physical properties of individual materials in solid and liquid state were considered as functions of temperature, and the transition between solid and liquid phase was programmed using smoothed Heaviside functions centered on fusion temperature T_f^i of the individual material:

$$\begin{aligned} k_i &= k_i^s + \left(k_i^l - k_i^s\right) flc2hs\left(T - T_f^i, dT\right) \\ \rho_i &= \rho_i^s + \left(\rho_i^l - \rho_i^s\right) flc2hs\left(T - T_f^i, dT\right) \end{aligned} \quad (6)$$

The latent heat of fusion of individual material L_i^f (J·kg^{-1}) was taken in account by means of equivalent enthalpy approach [8]:

$$C_p^{eq}{}_i = C_{p_i}{}^s + \left(C_{p_i}{}^l - C_{p_i}{}^s\right) flc2hs\left(T - T_f^i, dT\right) + + L_i^f \frac{exp\ \frac{-\left(T - T_f^i\right)^2}{dT^2}}{\sqrt{\pi}\, dT^2} \quad (7)$$

2.3. Deformed geometry

In the previous experimental study [4], after the cooling of the dissimilar joint the keyhole was not filled by the collapsing material, but remained empty, which confirms the important evaporative mass loss. This was the main motivation for use of Deformed Geometry formulation of moving mesh, which is the most suitable for the domain ablation because in this method the change of total volume implies the removal or addition of mass [9]. The ablation rate in the individual material was formulated as

$$V_i = \frac{q_{evap}}{\rho_i L_i^{vap}} \quad (8)$$

where L_i^{vap} is the evaporation heat (J·kg^{-1}), and applied as a normal mesh velocity to the top limit irradiated by the laser. The ablation rate dropped down to zero in the "cold" regions of the boundary, where normal mesh displacement was therefore suppressed, however, the vertical elongation of the mesh was still possible, which allowed the progressive sliding of the elements inside the digging keyhole. The transition between the evaporation rates of joined materials was programmed using smoothed Heaviside function:

$$V = V_1 + (V_2 - V_1)\, flc2hs(0 - x, dx) \quad (9)$$

The vertical limits of the domain had the condition dX = 0 and the mesh was allowed to slide along y axis freely. For the bottom domain, the condition dY = 0 was applied and the mesh could slide along x axis.

3. Use of COMSOL Multiphysics® Software

The present model involves *Heat Transfer in Solids* and *Deformed Geometry* modules that are strongly coupled and solved with time-dependent solver MUMPS on the workstation with Intel ® Xeon ® CPU E5-2699v4 (2 processors, 2.2 GHz, 44 cores) and 256 Gb RAM. The longest calculation needed about 2 h.

The main challenge of this numerical model consisted in avoiding the critical local deformation of mesh elements during the progression of the keyhole. Free tetrahedral fine mesh with double x-direction scale was applied over the domain (**Figure 1a**), to enhance the tolerance of the elements to the vertical squeezing. The 0.06 mm large meshes were generated on the top and lateral boundaries. A set of points with 0.0005 mm element size was created next to the top corners of the domain, where the elements underwent the most severe elongation during keyhole progression. The Yeoh smoothing was chosen for solving the deforming geometry problem because of the possibility to apply the stiffening coefficient to the mesh elements undergoing the deformation, which allows avoiding poor mesh quality and mesh inversion. By default, this value is considered as a constant. The application of stiffening coefficient over all solved domain slows down the calculation and makes the convergence a little more challenging, compared to the hyperplastic smoothing. However, the last one rapidly conducts to the mesh inversion. Therefore, it was decided to use Yeoh smoothing, but to program the global stiffening coefficient S_{Yeoh} as a function of local mesh displacement, accordingly to the critical regions observed during the deformation (**Figure 1b**):

$$\begin{aligned} S_{Yeoh} = s_{const}\, [&flc2hs(abs(dY) - 5e^{-4}, 2e^{-4}) + \\ &flc2hs(abs(dX) - 5e^{-4}, 2e^{-4}) + flc2hs(abs(x) - 1.7e^{-3}, 5e^{-4})] \end{aligned} \quad (10)$$

The dY-dependent Heaviside function activates the stiffening coefficient s_{const} in the meshes at the bottom of the keyhole and in the underlying material (**Figure 1c**), where the degradation of the element quality by squeezing is the most rapid and critical after reaching a certain vertical mesh displacement. Later, during the digging process comes the problem of excessive horizontal elongation of the meshes that form the part of top boundary that remains unaffected by laser beam (**Figure 1d**): therefore, the dX-dependent Heaviside function is activated when the horizontal displacement of meshes exceeds a certain level. Finally, close to the external vertical limits of the domain the stiffening is applied at all times as function of $abs(x)$. In this way, it was possible to avoid the harmful mesh deformations illustrated at the left of **Figure 1 c** and **d** that lead to the divergence of the calculation.

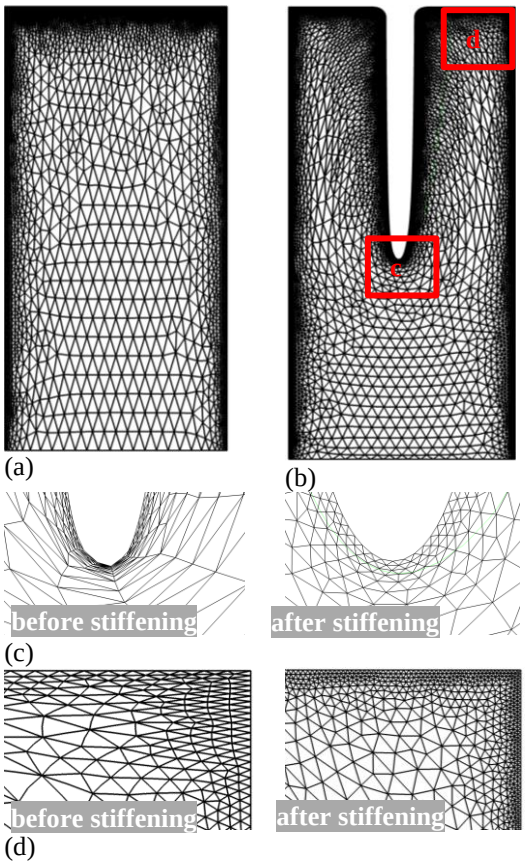

Figure 1. Initial (a) and deformed (b) geometry with details on elements quality at the bottom of the keyhole (c) and at the top corners of the domain (d) before (left) and after (right) the application of local stiffening.

The choice of additional numerical parameters is also important for better model convergence (**Table 1**). The spatial smoothening interval *dx* delimitates aluminum domain from magnesium domain. Taking in account that the total smoothing length for Heaviside function takes $2 \cdot dx$, the further increase of its value would suppress the effect of sharp change of properties across the joint line and would influence the shape of the keyhole. On the other hand, reducing *dx* down to µm level slows down the calculation and produces the convergence problems. For the temperature smoothing coefficient *dT*, a typical value for laser welding problems was used. The isotropic diffusion turning parameter $\delta_{id} = 0.4$ was used to fasten the convergence of heat transfer module; however, it did not diminish the maximal surface temperature limited by the vaporization temperature of considered materials. Finally, moving boundary smoothing turning parameter δ_{mds} of 0.5 allowed avoiding the convergence problems at the stage of keyhole initiation. In this way, the correct aspect of the mesh and easy convergence were attained even for high (up to ~10) depth to width ratio of the keyhole.

Table 1. Numerical parameters used in the model

Stiffening constant for Yeoh mesh smoothing	s_{const}	20	-
Spatial smoothening ½ interval	*dx*	0.1	mm
Temperature smoothening ½ interval	*dT*	100	K
Isotropic diffusion turning parameter	δ_{id}	0.4	-
Moving boundary smoothing turning parameter	δ_{mds}	0.5	-

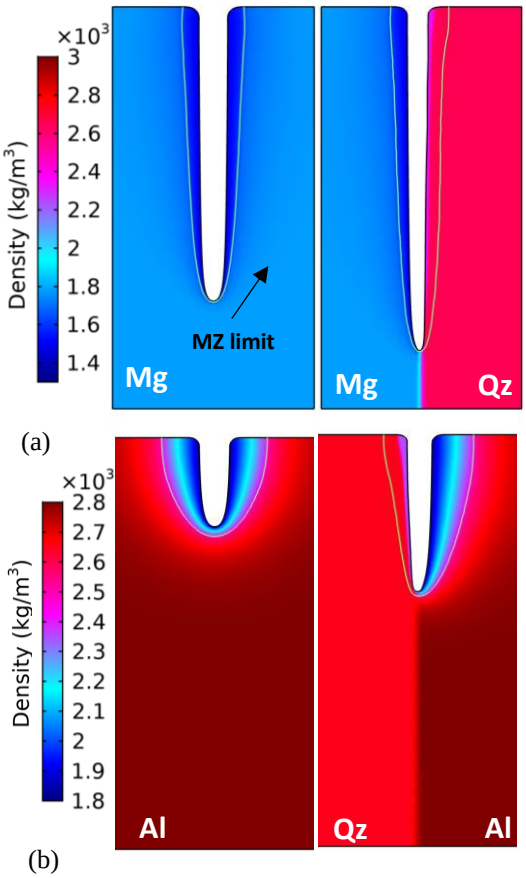

Figure 2. The effect of quartz addition to magnesium (a) and aluminum (b) on keyhole shape.

4. Experimental study

The experiments were performed using a pulsed Nd:YAG laser (λ =1064 nm), a focal distance of 200 mm and a focused spot diameter of 0.4 mm. Laser beam was centered at the interface between the 3 mm thick quartz sheet and the joint of the polished and rectified 3 mm thick magnesium AZ31 and aluminum A5754 alloy plates. No gas protection was used. A standalone pulse with parameters given in **Table 2** was applied in all experiments. Different values of beam offset from the joint line between two metallic plates on aluminum or magnesium side were applied, considered as negative in case of shift towards aluminum and positive in case of shift towards magnesium alloy. The details on high-speed imaging and sample preparation are described in [4]. Additionally, the melted zone dimensions in aluminum/quartz and magnesium/quartz couples were compared with dimensions of aluminum/aluminum and magnesium/magnesium couples (measured by DODO method [10]) to appreciate the effect of quartz sheet on the keyhole digging.

Table 2. Used laser parameters

Laser peak power	*P*	kW	2.5
Beam radius	*R*	mm	0.2
Pulse duration	t_{imp}	ms	6
Beam offset	Δ	mm	-0.3, -0.2, -0.1, 0, 0.1, 0.2, 0.3

5. Results and discussion

5.1. Role of frontal quartz window

To quantify the effect of quartz window on the observed keyhole shape, the calculations for 6 ms long pulse at the interface between individual metal and quartz plate were performed.

In case of magnesium **(Figure 2a)**, the keyhole was slightly deepened, and the quartz side remained practically unaffected by ablation, but presented a melted layer, which is in correspondence with experimental observations [4,5]. The contact with quartz window induced +1 mm increase in keyhole penetration, which is in good correspondence with experimentally observed average increase of +1.1 mm (**Figure 3a**).

In case of aluminum **(Figure 2b)**, the keyhole almost twice deep. The quartz was only slightly ablated and had a melted layer. A + 0.6 mm increase of keyhole penetration due to the contact with quartz was observed, compared to the experimentally observed average increase of +0.8 mm (**Figure 3b**). Such important effect of contact with quartz on aluminum can be attributed to the higher mismatch in thermal conductivities compared to magnesium (79 $W \cdot m^{-1} \cdot K^{-1}$) and 227 $W \cdot m^{-1} \cdot K^{-1}$ for magnesium and aluminum respectively and to 1.67 $W \cdot m^{-1} \cdot K^{-1}$ for quartz).

5.2. The keyhole features at aluminum/magnesium interface

In the first place, the calculated keyhole profiles were compared to the ablated areas formed at aluminum/magnesium joints after 6 ms laser pulse that were observed by SEM-EDX after the detachment of quartz window and to the keyholes observed in situ by HSI (**Figure 4**). The obtained numerical results reflect to the situation that would take place in absence of quartz window. The keyhole aspects in case of full laser beam offset on aluminum side (Δ = -0.3 mm) as well as in case of centered beam position and full laser beam offset on magnesium side (Δ = 0.3 mm) were globally reproduced.

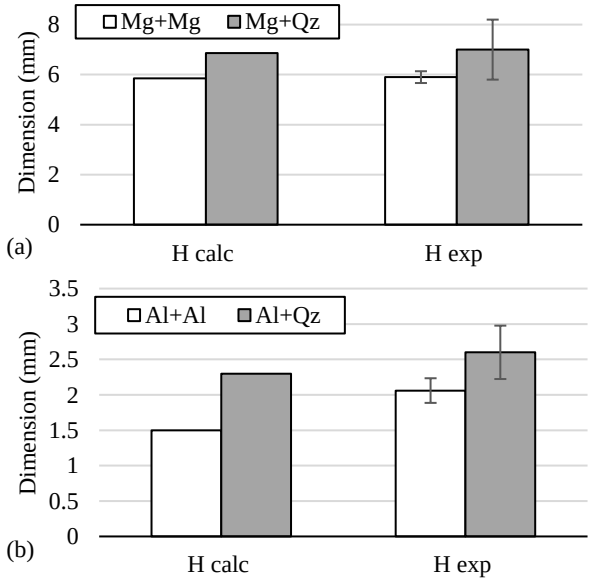

Figure 3. The effect of quartz addition to magnesium (a) and aluminum (b) on keyhole dimensions.

The difference between calculated and experimental widths of the keyholes W was ≤ 0.2 mm for all values of Δ, which is within the error range of the measurements on HSI videos [5] (**Figure 5a**). The keyhole penetration H was well reproduced for the centered beam position and 300 μm beam offsets on magnesium side (**Figure 5b**). The 300 μm offset on aluminum side resulted in 32% shorter keyhole compared to the experiment. The intermediate laser position $0<|\Delta|\leq R$ resulted in experimental weld penetrations similar to the centered beam case. This difference can be explained by the eventual gap between the plates and uncertain positioning of the beam, as well as by the influence of quartz window discussed in the previous section.

The cross-section areas of the keyholes S were in good correspondence with experimental results, with exception of $0>\Delta\geq R$ (offset on aluminum), where they seem underestimated (**Figure 5c**). The calculated ablated areas on magnesium side ($S_{calc}Mg$) showed correct correspondence with experimental areas (**Figure 5d**), when the calculated ablation areas in aluminum alloy ($S_{calc}Al$) at $0>\Delta\geq R$ were underestimated. Basing on the results described in 5.1, it can be supposed that experimentally observed ablation on aluminum side ($0>\Delta\geq 2R$) was promoted by the contact with quartz window.

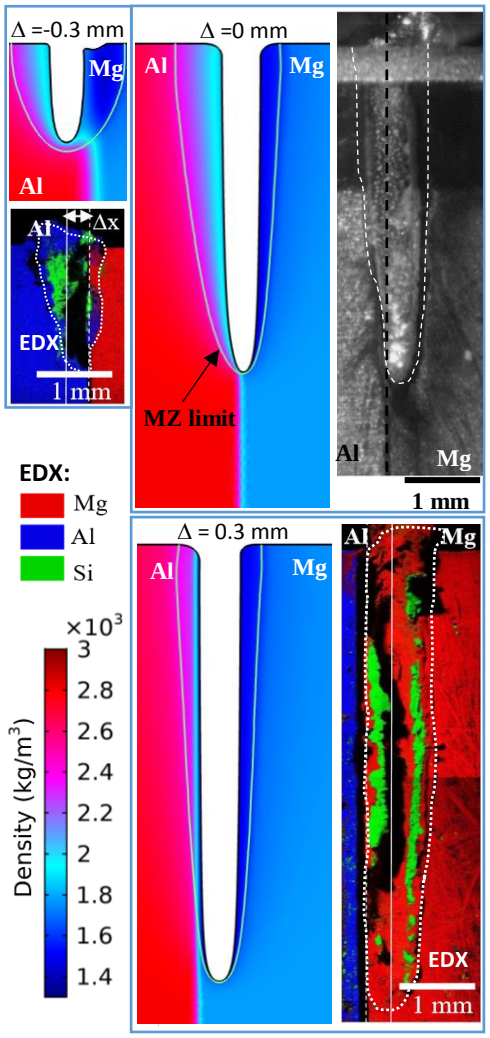

Figure 4. A comparison between calculated (density field) and experimental (EDX mappings [5], HSI image [4]) interaction zones in aluminum/magnesium joint.

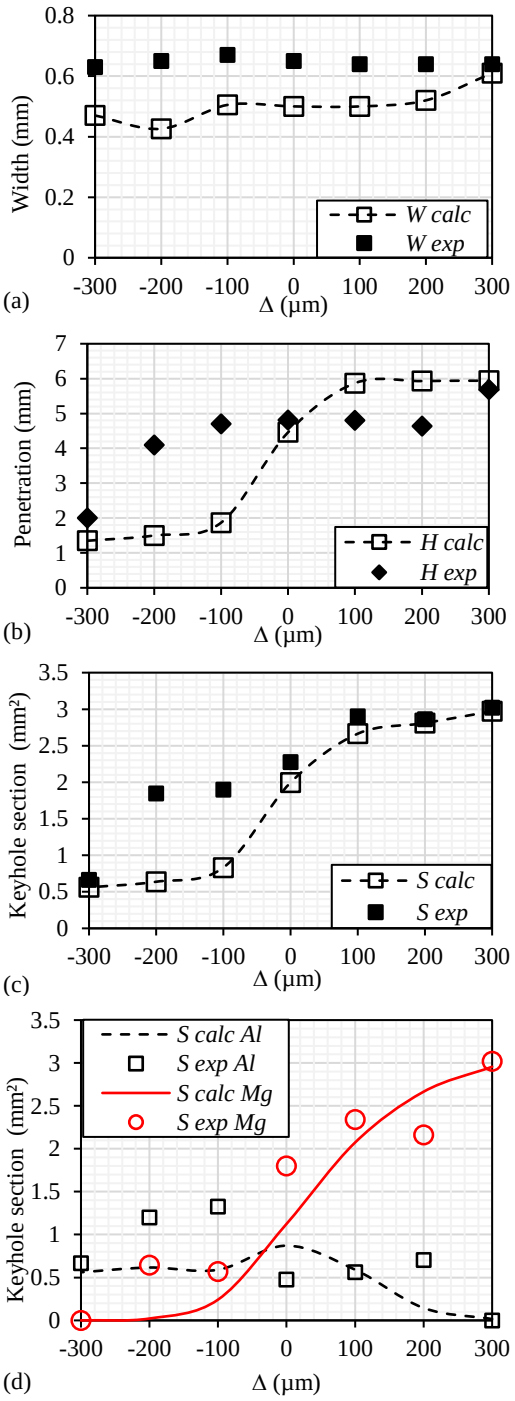

Figure 5. A comparison between calculated and experimental dimensions of the keyhole in aluminum/magnesium joint: (a) width, (b) penetration, (c) cross-section, (d) cross-section in each material.

6. Conclusions

A simplified 2D model of thermal ablation was applied to the case of laser-induced keyhole development at the dissimilar joint. The use of Yeoh smoothening method with stiffening coefficient applied in critical zones of the moving mesh allowed attaining easy convergence for high depth to width ratio of the keyhole.

The model was able to correctly reproduce the keyhole dimensions in case of homogenous and binary metal/quartz combinations and allowed estimating the effect of quartz on the keyhole penetration. Aluminum alloy developed much deeper keyhole in presence of quartz, therefore the observation of the keyhole in aluminum and its alloys through the quartz window suffers from important deformations. The relative deepening of the keyhole in magnesium was much lower.

In case of aluminum/magnesium metal combination, the model renders the keyhole evolution with laser offset from the joint line that would take place in absence of quartz window. In case of centered beam position, the mismatch in vaporization temperatures induced the preferential formation of deep and thin keyhole on magnesium side. The displacement of the keyhole on magnesium induced further slight increase of penetration, when the displacement on aluminum reduces abruptly the keyhole.

7. References

[1] Torkamany, M.J., Malek Ghaini F., Poursalehi, R., An insight to the mechanism of weld penetration in dissimilar pulsed laser welding of niobium and Ti-6Al-4V, *Optics and Laser Technology*, **79**, 100-107 (2016).

[2] Grevey, D., Vignal, V., Bendaoud, I., Erazmus-Vignal, P., Tomashchuk, I., Daloz, D., Sallamand, P., Microstructural and micro-electrochemical study of a tantalum–titanium weld interface, *Materials & Design*, **87**, 974-985 (2015).

[3] Tomashchuk, I., Assemblage hétérogène cuivre-inox et TA6V-inox par les faisceaux de haute énergie : compréhension et modélisation des phénomènes physico-chimiques, phD thesis at Université de Bourgogne, France (2010). http://www.theses.fr/2010DIJOS055

[4] Tomashchuk, I., Mostafa, M., Caudwell, T., Sallamand, P., Duband, M., Behavior of laser induced keyhole during dissimilar welding of metals, *Lasers in Manufacturing Conference 2017*, June 26-29, Munich, Germany (2017).

[5] Tomashchuk, I., Mostafa, M., Caudwell, T., Sallamand, P., Duband, M, Formation du capillaire de vapeur lors de l'interaction de laser de puissance avec la jonction dissimilaire Al-Mg, *Congrès Français de Thermique 2017*, 30 mai – 2 juin, Marseille, France (2017).

[6] Matsunawa, A., Seto, N., Kim, J.D., Mizutani, M., Katayama, S., Observation of keyhole and melt pool behavior in high power laser welding, *Transactions of JWRI*, **30**-1, 13 (2001).

[7] Frei, W., Modeling Thermal Ablation for Material Removal, *Comsol blog*, March 30 (2016).

[8] Bonacina, C., Comini, G., Fassano, A., Primicerio, M., Numerical solutions of phase change problems, *International Journal of Heat Mass Transfer*, **16**, 1825-1832 (1973).

[9] Frei, W., Model Translational Motion with the Deformed Mesh Interfaces, *Comsol blog*, September 4 (2015).

[10] Schneider, M., Perçage profond par laser : Analyse des processus physiques. phD thesis at Université Pierre et Marie Curie - Paris VI, France (2006). https://tel.archives-ouvertes.fr/tel-00271589

8. Acknowledgements

The authors would like to thank the Government of Egypt for funding the postdoctoral fellowship of Massaud Mostafa and to Dr Loïc Renversade from COMSOL support for his kind advices on use of Deformed Geometry module.